FORMATION OF Cu-RICH NANOPRECIPITATES IN Cu CONTAINING PEARLITIC SGI

Laura N. García
Instituto de Mecánica Aplicada, Universidad Nacional de San Juan, San Juan, Argentina

Rodrigo Magnabosco
Departamento de Engenharia de Materiais, Centro Universitário FEI, São Bernardo do Campo, Brasil

Roberto E. Boeri
Instituto de Investigaciones en Ciencia y Tecnología de Materiales, Universidad Nacional de Mar del Plata-CONICET, Mar del Plata, Argentina
CONICET, Ciudad Autónoma de Buenos Aires, Argentina

Alfredo J. Tolley
Centro Atómico Bariloche, Comisión Nacional de Energía Atómica, San Carlos de Bariloche, Argentina
CONICET, Ciudad Autónoma de Buenos Aires, Argentina

Marcela E. Saavedra
ICATE-CONICET, San Juan, Argentina
CONICET, Ciudad Autónoma de Buenos Aires, Argentina

https://doi.org/10.1007/s40962-020-00543-x

Abstract

The presence of Cu-rich nanoprecipitates in a pearlitic spheroidal graphite (ductile) cast iron alloyed with 0.82 wt%Cu was studied. The size and distribution of the precipitates were examined by transmission electron microscopy at different locations of the pearlitic matrix. Some areas were nearly free from precipitates, while other regions showed precipitates at the cementite and ferrite lamellae and at the ferrite/cementite interface. Calculation of the thermodynamic equilibrium under stable and metastable conditions using Thermo-Calc led to the identification of the conditions controlling the formation of Cu-rich nanoprecipitates along three different stages depending on the Cu concentration. Together with a differential scanning calorimetry test and elemental diffusional calculations, thermodynamic predictions supported the observation of Cu-rich precipitates despite the low concentration of Cu of the alloy investigated and allowed the authors to explain the observed heterogeneity in the distribution of precipitates as resulting from the heterogeneous distribution of Cu in the alloy caused by microsegregation during solidification. The knowledge gained is relevant for the design of strengthening strategies in SGI based on the dispersion of Cu-rich nanoprecipitates.

Keywords: *spheroidal graphite cast irons, Cu-rich nanoprecipitates, nanostructured materials, Thermo-Calc, microsegregations, transmission electron microscopy*

Introduction

Nanostructured materials are essential for the modern world, as their continuous innovation is critical for increasing the mechanical resistance of materials for structural use, with the consequent reduction in the volumes required in different applications, contributing to a more sustainable future.[1] In this regard, the fine dispersion of nanoparticles has proven to be one of the most effective methods for improving the strength of ferrous alloys.[2] In particular, the formation of Cu-rich nanoprecipitates in

Received: 09 September 2020 / Accepted: 26 October 2020 / Published online: 29 November 2020

steels has become an attractive method to increase strength without causing a significant reduction in ductility at a relatively low cost.[3,4] As a result, steels containing Cu-rich precipitates have been extensively studied. The precipitation is driven by the negligible solubility of Cu in iron at room temperature. Therefore, Cu-rich particles may form in the ferrite matrix at some stage of cooling or during isothermal stages. The Cu- rich phase has been described as a solid solution of Fe in the Cu FCC unit cell and was designated as ε.[5] Furthermore, the presence of other alloying elements has been shown to affect some characteristics of the Cu-rich nanoprecipitates, such as their chemical composition, size and dispersion.[3,6]

In contrast, there are few studies dedicated to the investigation of Cu-rich nanoprecipitates in cast irons. Bataev et al.[7] studied their precipitation in the pearlitic structure of grey cast irons with Cu contents between 1.6 and 10.8 wt% using transmission electron microscopy (TEM). They detected their presence at the cementite/ferrite interface and linked it to an increase in the microhardness. Razumakov et al.[8] found these nanoprecipitates in cast irons with Cu contents higher than 3 wt% and also associated them with an increase in the microhardness. Bataev et al.[9] found them in cast irons with 14.7 wt%Cu and performed microhardness measurements for different Cu contents, concluding that microhardness experienced a decline for cast irons with Cu contents between 10 and 11 wt%Cu. Finally, Bataev et al.[10] studied white cast irons alloyed with Cu and Al, detecting the nanoprecipitates only when the Cu content was higher than 3 wt% and concluded that they precipitated during austenite decomposition.

For spheroidal graphite cast irons (SGI from now on), the investigation of the Cu effect has been focused on the understanding of its role as pearlite promoter. This has been done by studying the influence of Cu on the ferrite and pearlite fractions, on the eutectoid temperatures and on the carbon diffusion coefficient.[11–15]Usually, when a pearlitic matrix is desired in these Fe–C–Si alloys, 0.2 up to 0.4 wt% Mn levels are combined with Cu levels between 0.6 and 1 wt%.[12,14] Although these low Cu concentrations might not be considered high enough to promote the precipitation of Cu-rich phases,[7–10] a recent study found the presence of Cu-rich nanoprecipitates in a pearlitic SGI alloyed with 2.72 wt%Si, 0.5 wt%Mn and 0.82 wt%Cu.[16] The authors attributed the presence of these nanoprecipitates to the microsegregation developed during solidifications of SGI, which causes the austenite to be heterogeneous.[12,13,17,18]While Si and Cu—graphitizing elements—tend to segregate toward the first-to-freeze (FTF) zones, Mn—a carbide stabilizing element—tends to concentrate in the residual liquid, i.e., into the last-to-freeze (LTF) zones.[19]

This investigation aims at examining the presence of Cu-rich nanoparticles in SGI alloyed with a low amount of Cu. The precipitates were revealed by TEM studies. Thermo-Calc thermodynamic calculations [20] using TCFE9 database are used to assess the feasibility of non-isothermal precipitation of Cu-rich nanoprecipitates, accounting for the influence of the microsegregation pattern present in austenite. Finally, the transformation of austenite into pearlite is investigated by differential scanning calorimetry (DSC) to assess the possibility of Cu to diffuse during pearlite growth and during cooling down to room temperature.

Materials and Methods

The study was carried out on samples taken from an as-cast SGI alloy having the composition listed in Table 1, as determined by a spark optical emission spectrometer. The same alloy was used in a previous study aimed at investigating the partition of Cu between ferrite and cementite.[16]

The melt was produced in a medium-frequency induction furnace with a capacity of 1500 kg. SAE 1010 steel scrap, foundry returns and pig iron were used as raw materials. Ground graphite, Si_2Ca and FeSi were employed in order to adjust the C and Si concentrations in the melt. Subsequently, the base metal was overheated to 1650 °C for 20 min. The sandwich method was used to complete the nodularization procedure with 1.5 wt% of Fe–Si–Mg–Ce. For the inoculation, 0.7 wt% of fine FeSi (75 wt%Si) was added in the reaction ladle. Finally, the melt was poured into a ladle to fill Y-block-shaped green sand molds to obtain 1-inch Y-blocks according to the ASTMA536-84 standard. The cooling rate was recorded (Figure 1), averaging 20 °C/min between 900 and 800 °C.

The microstructure of as-cast samples consisted of 10% graphite, 11% ferrite and 79% pearlite (percentages per unit area). In order to determine these percentages, the commercial software MATERIALS PLUS was used on 100X optical microscopy images. The standard deviations were calculated from five measurements as 1.4, 1.9 and 3.2%, respectively. An example is presented in Figure 2.

Table 1. Composition of the SGI Sample Studied in this Work [Values in wt%]

Element	C	Si	Mn	P	S	Cr	Cu	Sn	Mg	Al	CE
Concentration	3.58	2.72	0.5	0.02	0.01	0.03	0.82	0.02	0.05	0.01	4.49

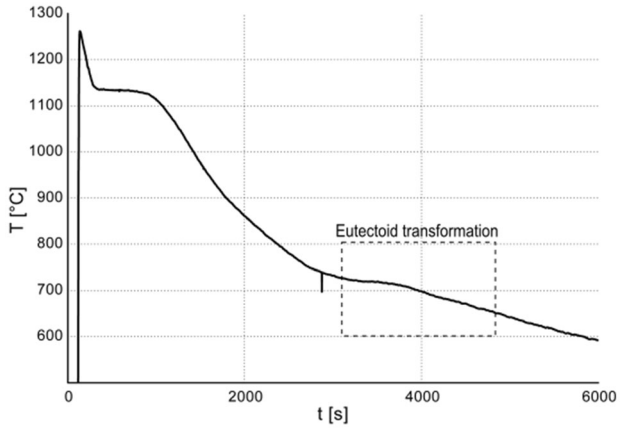

Figure 1. Recorded cooling curve. The section corresponding to the eutectoid transformation has been highlighted.

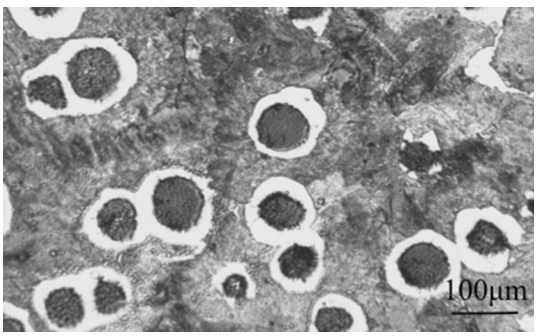

Figure 2. Microstructure of the pearlitic SGI sample considered in this study.

The metallography was prepared by conventional polishing and etched with 5% Nital. The nodule count averaged 100 nodules/mm^2, the nodularity 80% and the average nodule diameter was 25 µm. The nodularity of the sample was determined by comparison to standard charts.

The alloy was examined making use of a FEI Tecnai F20 transmission electron microscope (TEM) operated at 200 kV equipped with a Schottky field emission gun and an EDAX Apollo Energy Dispersive Spectroscopy (EDS) unit. Under these experimental conditions, a spatial resolution for EDS analysis of 1nm is achievable. The TEM samples were prepared by mechanical grinding to about 200 µm thickness, followed by dimple grinding combined with ion milling using a precision ion polishing system. The chemical composition at selected positions or phases was measured by EDS using the Cliff-Lorimer method with calculated k_{AB} factors. As a result of the uncertainty in the k_{AB} factors, the results do not provide a reliable quantification of the chemical composition of the phases examined but are suitable as a fair semi-quantitative measurement.[21]

In addition, the equilibrium phase fractions as well as their composition were simulated with Thermo-Calc and TCFE9 database for different temperatures and alloying concentrations. The presence of other alloying elements besides Si, Mn and Cu was ignored to simplify the calculations. This assumption is valid because the concentration of other alloying elements is low enough to have a negligible effect on the phase transformations. The simulations were carried out for the nominal composition of the alloy (Table 1) as well as for the estimated local composition at the FTF and LTF zones.

Although the predictions from equilibrium thermodynamic calculations might not represent thoroughly the transformations resulting after continuous cooling, they can be used to assess the potential precipitation of Cu-rich phases.

Finally, a 3-mm-diameter sample was prepared and tested with DSC to identify the onset and completion of the pearlitic transformation during the cooling of austenite. The DSC was temperature and heat-flux calibrated by comparing the temperature and fusion enthalpies of In, Sn and Al. The cooling gas was Ar at 30 mL/min and 1 atm. The thermal cycle consisted of heating the sample at 20 °C/min up to 950 °C, where it was isothermally held for 20 minutes and then cooled at 20 °C/min to room temperature. The heating rate was arbitrarily chosen since Ivanova et al.[22] concluded that it does not play an important role in the final microstructure. The time at the austenitization temperature was aimed at reaching the equilibrium redistribution of C[23] without altering the distribution of substitutional elements.[24] The cooling rate was chosen to be similar to that recorded during the cooling of the samples after casting. Under these experimental conditions, the temperatures delimiting the pearlite transformation measured in the DSC curves should be very similar to those produced during the cooling stage after solidification.[23] To determine the limit temperatures, the first derivative of the DSC signal was considered. A Savitzky Golay filter was used to smooth the DSC signal.

Results and Discussion

The microstructure of a pearlite colony is shown in Figures 3 and 4. As the samples were not prepared by FIB thinning or a method that enables the selection of the area to study, we cannot with certainly affirm that the recorded areas correspond to FTF or LTF zones. Even for a completely pearlitic sample, heterogeneities are present throughout the matrix.

The pearlite interlamellar spacing was measured on the pearlite colonies shown in Figures 2 and 3, resulting in an average value of 300 nm. In all cases, spheroidal particles of about 10 to 60 nm in diameter appear in different locations: inside ferrite and cementite lamellae and at the ferrite/cementite interface. In Figure 3a, precipitates are distinguished inside the ferrite lamellae and some inside the cementite, whereas in Figure 3b precipitates inside the

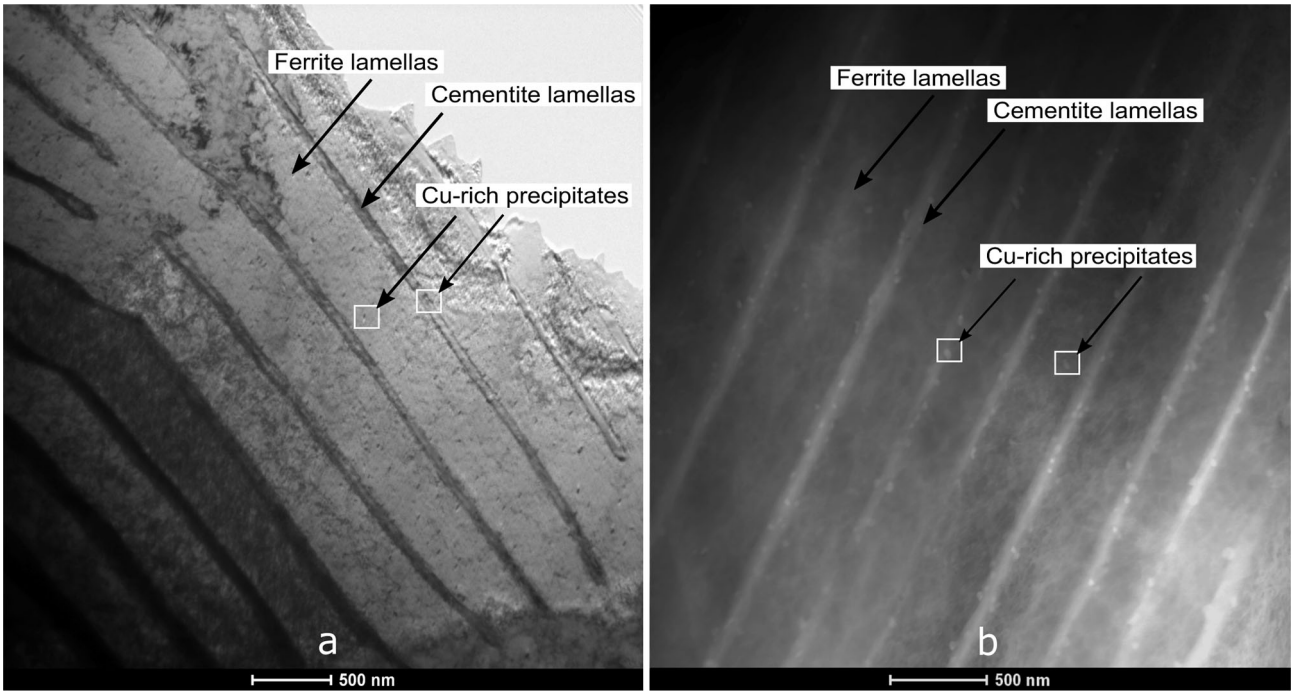

Figure 3. Cu-rich precipitates in a pearlite colony: (a) TEM bright-field and (b) TEM dark-field images.

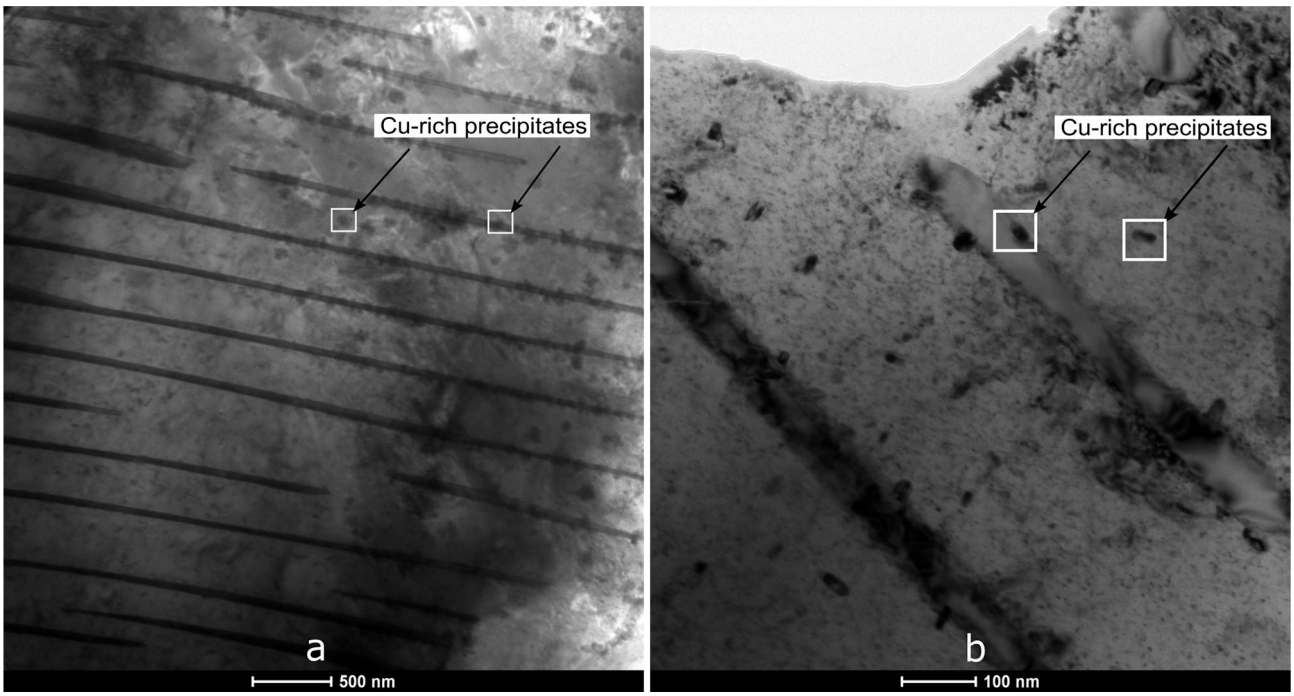

Figure 4. Cu-rich precipitates in a pearlite colony: (a) TEM bright-field image showing the heterogeneous dispersion of precipitates within a pearlite colony and (b) higher magnification TEM image revealing precipitates at the ferrite/cementite interface and inside the lamellae.

cementite as well as at the interface are evident. In both cases, they are homogeneously distributed. In Figure 4a, the size and distribution of the precipitates change in comparison with the formerly presented colonies (Figure 3). Precipitates are predominantly located in some areas of the examined field, reaching sizes of up to 60 nm, while other areas of the same field are nearly free from precipitates. Finally, in Figure 4b the precipitates are mostly located at the ferrite/cementite interface.

The understanding of the location of the precipitates calls for a careful analysis of the precipitation process. Three different stages for Cu-rich phase precipitation were proposed:

(1) During austenite cooling. According to Bataev et al.,[9] when precipitates are present in both ferrite and cementite lamellae, they must have formed in austenite during cooling.
(2) During pearlite growth. In this case, both, the austenite/ferrite/cementite triple junction, as well as the austenite/cementite and austenite/ferrite interface would be preferential locations for the precipitates' nucleation. The later would explain their presence in ferrite lamellae.
(3) During cooling after pearlite growth has finished, as ferrite becomes supersaturated in Cu.

The chemical composition of the precipitates is listed in Table 2. The values are the average of ten analyses. Since the volume of the material that generates the characteristic X-rays is larger than the nanoprecipitates, Fe, Si and Mn counts could be coming from the surrounding matrix. Therefore, the chemical composition of the precipitates cannot be determined precisely. Nevertheless, it is certain that the nanoprecipitates composition consistently shows a high concentration of Cu. Both the examination of the microstructure and the EDS analyses prove with no doubt that Cu-rich precipitates form in the alloy after a relatively slow post-solidification cooling stage inside a sand mold, as confirmed in recent investigations.[16] However, most of the existing literature has not identified Cu-rich precipitates in cast irons containing relatively low concentrations of Cu. The understanding of the precipitation of Cu-rich phases in the alloy under investigation can be supported by thermodynamic calculations of phase equilibrium at different temperatures.

The phase transformations during cooling after solidification of Fe–C–Si alloys leading to cast iron with graphite and a pearlitic matrix are governed by the stable Fe–C–Si diagram at high temperatures (liquid-austenite-graphite equilibrium), but react according to the metastable equilibrium (austenite-ferrite-cementite) at lower temperatures.[13] The first stage of the analysis of the presence of Cu-rich precipitates focuses on the equilibrium at higher temperatures. Therefore, a stable equilibrium Fe–Cu isopleth section was calculated with Thermo-Calc for the nominal concentrations of C, Si and Mn (Figure 5). It is evident that Cu solubility decreases in austenite (FCC_A1) as well as in ferrite (BCC_A2) with temperature. The precipitation of a Cu-rich phase can take place over three different temperature ranges. For alloys with concentrations of Cu lower than approximately 1.3 wt%, the precipitation of a Cu-rich phase (FCC_A1#2) is expected to take place in ferrite as the temperature drops and the maximum solubility of Cu in ferrite diminishes. Therefore, for the nominal Cu concentration of the alloy under study (0.82 wt%), precipitation under equilibrium conditions is possible only below 700°C. This is also confirmable from Figure 6, where the volume percentage of each phase is shown for the nominal composition of the alloy. From Figure 4, when Cu concentration exceeds 1.3 and up to 2.5 wt%, the Cu-rich phase can begin to form simultaneously with ferrite during the decomposition of austenite and will proceed during further cooling of ferrite. Only when Cu concentration exceeds 2.5 wt%, Cu-rich precipitates can start forming during austenite cooling.

Table 2. EDS-TEM Analysis of the Nanoprecipitates [Values in wt%]

Element	Si	Mn	Cu	Fe
Averaged concentration	1.4	1.1	26.9	70.6
Standard deviation	0.1	0.4	0.5	0.2

When the metastable Fe–Cu isopleth section is explored instead (Figure 7), the solubility of Cu in both austenite as well as in ferrite diminishes. Therefore, the three precipitation stages of a Cu-rich phase described above for the stable equilibrium calculations will take place in this case along different concentration ranges. Precipitation can start from the austenite for Cu concentrations greater than 1.5 wt%Cu. It may take place simultaneously with ferrite and cementite for Cu concentrations between 0.95 and 1.5 wt%, and it will only occur in ferrite for a Cu concentration below 0.95 wt%. It is difficult to assess with certainty the temperature at which the transformations begin to take place according to the metastable equilibrium. Nevertheless, the absence of free cementite in the microstructure and the very small presence of free ferrite suggest that the transition from stable to metastable equilibrium has taken place approximately at the temperature of the start of austenite transformation into ferrite and cementite. This takes place approximately between 850 and 830 °C according to Figure 7, depending on the concentration of Cu. Therefore, all discussions from this point forward will assume that C transport from the austenite to the graphite ceased at about 830 °C. These calculations also show that the precipitation of the Cu-rich phase can take place at different stages of transformation/cooling, depending on the local concentration of Cu. Therefore, the microsegregation of Cu generated during solidification could have an impact on the size and distribution of such precipitates. This matter will be discussed below.

The Cu content of the Cu-rich precipitates (FCC_A1#2) as predicted by Thermo-Calc is 100 wt%Cu. This diverges from the results of the EDS-TEM (Table 3). Nevertheless, it has been already stated above that the results of Table 2 do not represent a precise analysis but a manifest tendency of the precipitates to be richer in Cu.

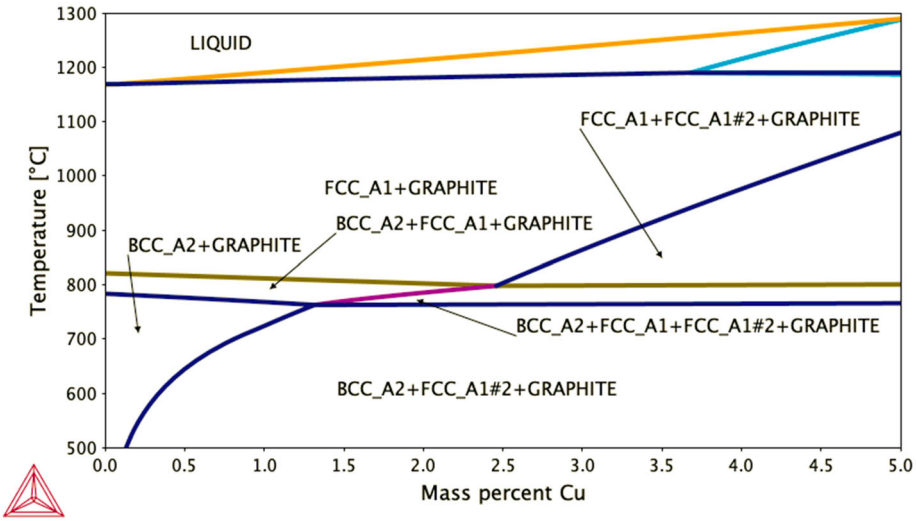

Figure 5. Stable isopleth section for the nominal composition of the alloy.

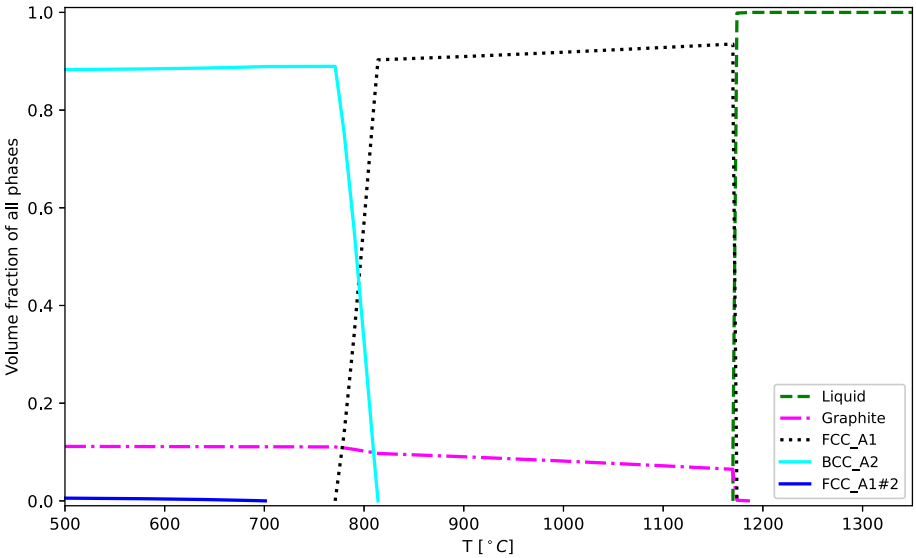

Figure 6. Volume fraction of the stable equilibrium phases during solidification and further cooling of the alloy for its nominal composition.

In order to understand the consequence of the heterogeneities developed during solidification and then inherited by the austenite phase, alloying element concentrations were estimated at the FTF and LTF areas from the nominal bulk concentrations. For that aim, the Scheil equation was used, as it suitably represents the development of heterogeneities during the solidification of SGI.[13] Its expression is given by:

$$C_s = kC_0(1-g)^{k-1} \qquad \text{Eqn. 1}$$

where C_s is the solute concentration in the solid, k is the equilibrium segregation coefficient, C_0 is the initial concentration and g is the solid fraction. C_0 was considered as the nominal concentrations reported in Table 1 corrected by a factor of 1.05 to account for graphite precipitation during solidification.[13] The Si, Mn and Cu equilibrium partitioning coefficients proposed by Boeri et al.[19] were utilized, and the cooling rate effect was ignored as little deviation from Scheil predictions is expected when cooling rate varies.[24] The FTF zones solute concentrations were then calculated from the Scheil equation assuming $g = 0.01$, and the LTF areas segregations with $g = 0.9$, i.e., 10% remaining liquid. The results of the calculated solute concentrations at the FTF and LTF areas of the matrix are listed in Table 3. At the FTF, Cu and Si concentrations are greater than the average concentration, while Mn concentration is lower.

Figures 8a and 7b show the volume fraction and the predicted temperatures for the formation of different phases when graphite precipitation is suspended so that cementite could appear, i.e., under metastable equilibrium. These

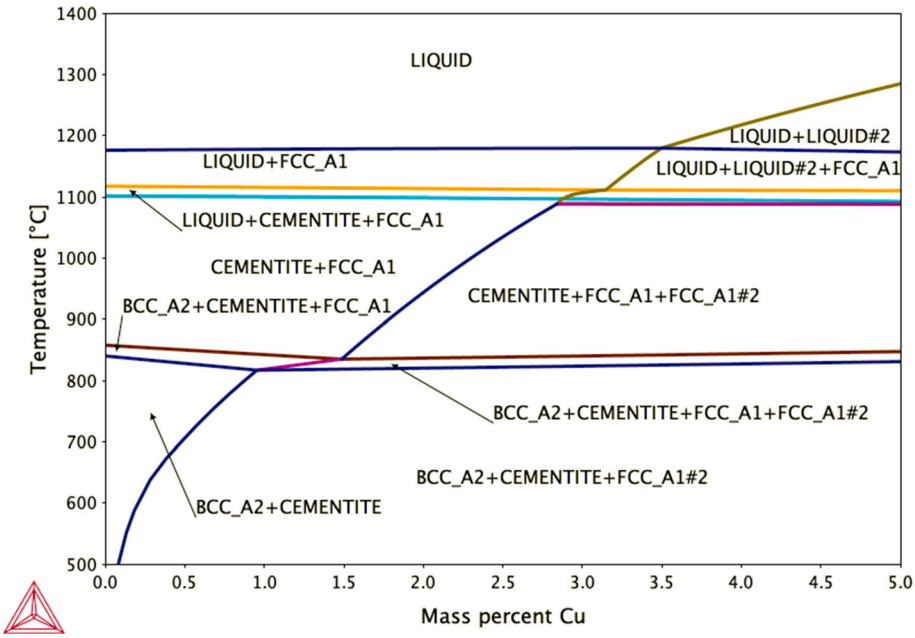

Figure 7. Metastable isopleth section for the nominal composition of the alloy.

Table 3. Concentrations Computed for the FTF and LTF Zones [Values in wt%]

Element	Si	Mn	Cu
FTF	3.1	0.4	1.2
LTF	2.5	0.7	0.5

simulations correspond to the nominal composition of C, and the concentrations of Si, Mn and Cu at the FTF and LTF zones, respectively. According to Figure 8a, the precipitation of the Cu-rich phase at FTF begins at temperatures above those corresponding to pearlite formation and continues as cooling proceeds. Therefore, the particles observed by TEM could have been formed at any of the three precipitation stages described above. On the other hand, when calculations are made accounting for the chemical composition at the LTF areas, as in Figure 8b, the precipitation of Cu-rich phases can occur only after the pearlitic transformation has been completed. While pearlite transformation takes place between 830 and 820 °C, the Cu-rich phase precipitation occurs below 750 °C. Another important fact is that the volume of the Cu-rich phase increases with Cu content. Then, under equilibrium conditions, a greater volume of precipitates is expected at the FTF as compared to LTF zones. This provides a reasonable explanation for the metallographic observations, where different densities of precipitates were found in different locations in the pearlitic matrix.

During pearlite growth, Cu partitions to ferrite, as it cannot be dissolved in cementite (TCFE databases assumes no solubility of Cu in cementite, in line with this statement). This partitioning behavior was verified in earlier work,[16] where the Cu concentration in cementite was found to be 4.5 times smaller than that measured in ferrite. Therefore, during pearlite growth Cu will be rejected to the austenite in front of cementite. This high Cu concentration could induce the precipitation of Cu-rich nanoparticles right in front of the cementite/austenite interface or at the triple junction austenite/ferrite/cementite. This is a feasible scenario for the Cu-rich composition in the FTF zone. On the other hand, when the local composition is that of the LTF zone, Cu-rich particles are not favored to nucleate, and Cu could be redistributed in austenite, to be then included in the growing ferrite. This explanation of the precipitation of Cu-rich particles is supported by previous work [16] which concluded that Cu atoms would find a faster diffusion path away from the cementite/austenite interface along the austenite/pearlite interface, being the triple conjunction austenite/ferrite/cementite a preferential nucleation site. Therefore, the precipitates observed along the ferrite/cementite interface will have probably formed during pearlite growth. Precipitates found inside cementite lamellae were formed right ahead of the growing cementite/austenite interface as a result of Cu rejection. They appear inside cementite lamellae because they are engulfed by cementite as it grows. Finally, Cu-rich precipitates inside ferrite lamella are most probably formed during the cooling of the pearlite after the pearlitic transformation is completed, as the Cu solubility in ferrite decreases.

In order to assess the possibility of Cu to diffuse and form the nanoprecipitates during cooling, it is necessary to identify the actual temperatures of pearlitic growth. The pearlitic transformation was examined by DSC. The differential calorimetry plot is shown in Figure 9. Typically,

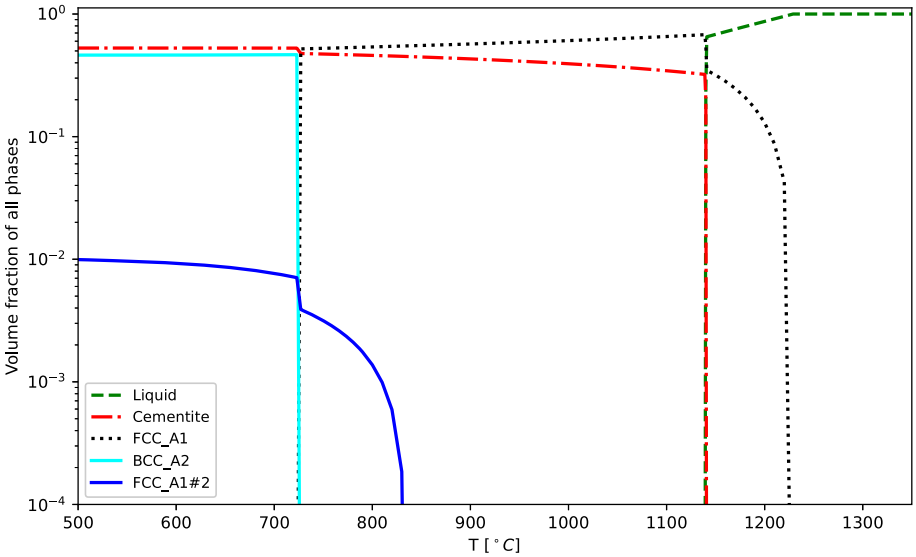

a

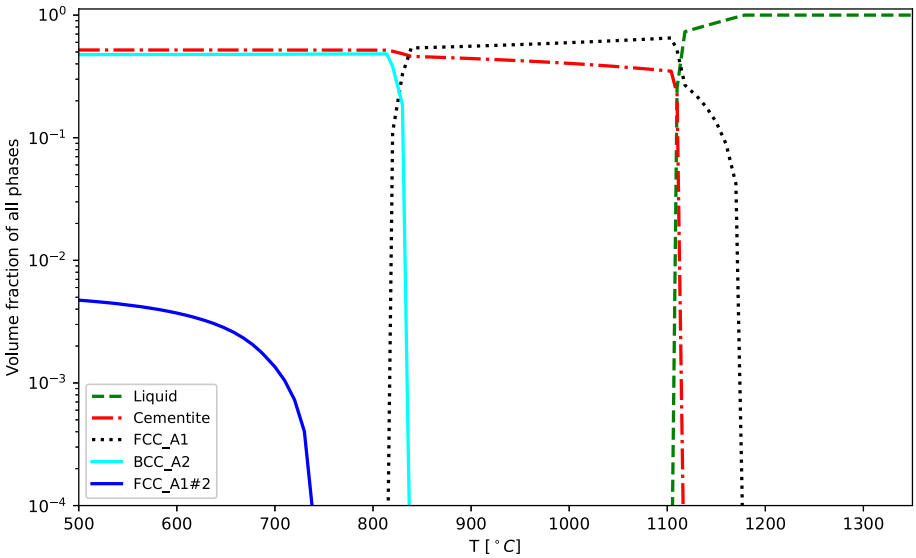

b

Figure 8. Volume fraction of the metastable equilibrium phases during solidification and further cooling of the alloy for the estimated composition at the (a) FTF and (b) LTF zones.

two exothermic transformations are found during cooling: austenite decomposition to ferrite and graphite, and austenite decomposition to pearlite.[22] Nevertheless, as the sample matrix is mainly pearlitic, the amplitude of the inflection in the curve caused by the ferritic transformation is almost negligible when compared to that corresponding to the pearlite growth onset. This explains the characteristics of the plot in Figure 9, where only one peak is distinguished.

The first derivative is also plotted in Figure 9 to identify the starting and completion temperatures of the exothermic peaks associated with pearlite transformation: 722 and 660 °C, respectively. At a cooling rate of 20 °C/min, the pearlite transformation took a total time of 186 s. For a pearlite colony average size of 60 μm,[16] the pearlite front velocity can be estimated a v = 0.3 μm/s . This growth rate can be accounted for to assess the extent of Cu redistribution in austenite during austenite/pearlite front progress.

Murakami et al.[25] proposed that the diffusion coefficient of Cu in austenite is given by:

$$D^{\gamma}_{Cu} = 4.34 \times 10^{-5} \exp\left(-\frac{280000}{RT}\right) \left[m^2/s\right] \qquad \text{Eqn. 2}$$

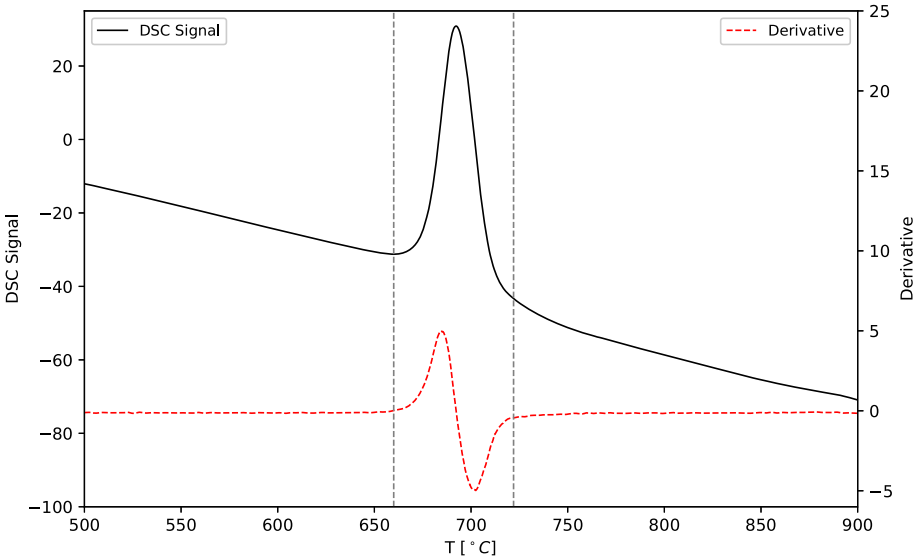

Figure 9. DSC curve for a cooling rate of 20 °C/min and its derivative. The starting and completion temperatures of the pearlitic transformation are identified.

They also estimated the interfacial diffusion coefficient by considering the activation energy for interfacial diffusion as half of that corresponding to lattice diffusion.[26] Then the interfacial diffusion coefficient is:

$$D^{\gamma}_{Cu} = 4.34 \times 10^{-5} \exp\left(-\frac{280000}{2RT}\right) \left[m^2/s\right] \qquad \text{Eqn. 3}$$

The lattice diffusion coefficients for high temperatures calculated with (2) are in good agreement with the experimental results compiled by Fridberg et al.[27]

At the upper limit of pearlite transformation temperature (722 °C), the diffusion coefficient calculated with (2) is $D^{\gamma}_{Cu} = 8.6 \times 10^{-20} m^2/s$, then the diffusion distance calculated as $x = D^{\gamma}_{Cu}/v$, $x = \left(D^{\gamma}_{Cu} t\right)^{1/2}$ where v is the pearlite front velocity, determined to be less than 1nm, suggesting that Cu migration would be negligible during pearlite growth. Nevertheless, if interfacial diffusion is accounted for, the diffusion coefficient calculated is $D^{\gamma}_{Cu} = 1.9 \times 10^{-12} m^2/s$ and the diffusion distance is $x = 6 \times 10^3$ nm. Therefore, in this case, Cu redistribution would be possible during the growth of pearlite under the current experimental conditions, from the cementite front to the ferrite front (200 μm approximately), enabling the precipitation of Cu-rich phases.

Although the formation of Cu-rich precipitates during pearlite growth depletes Cu atoms from ferrite, there is still a high Cu concentration in solution, at least 1 wt%Cu[16], which is above the Cu solubility limit in this phase at room temperature (Figure 7). Therefore, the next step is to assess the feasibility of Cu-rich phase precipitation during pearlite cooling after the pearlitic transformation is completed.

The DSC analysis has shown that the pearlitic transformation ends at 660 °C. The diffusion coefficient of Cu in ferrite at 660 °C as compiled by Fridberg et al.[27] is $D^{\alpha}_{Cu} = 3 \times 10^{-19} m^2/s$, which is high enough to enable nanometric diffusion of Cu atoms to enlarge the existing precipitates and/or to form fresh precipitates inside the ferrite lamellae. Nevertheless, this postulation needs additional investigation, as the diffusion coefficient decreases with temperature. In any case, the decrease of Cu solubility in ferrite can result in the ejection of Cu and further formation of precipitates.

In summary, this investigation has proved that the recently identified presence of Cu-rich precipitates in SGI alloyed with small amounts of Cu is clearly supported by thermodynamic and elemental diffusional calculations. Additionally, the uneven distribution of precipitates has been explained as resulting from the typical microsegregation of solutes present in SGI.

The results suggest that the use of Cu as a strengthening agent by nanoprecipitation should be limited to low concentrations since higher contents of Cu will produce a greater volume of the Cu-rich phase, but, as this increased volume will form at a higher temperature during cooling of austenite, the particles will probably be coarser and, therefore, have little influence on strengthening. In addition, the results imply that the chemical composition of SGIs, that is, the concentration of Si, Mn and other alloying elements, can be optimized to produce the largest possible volume fraction of fine Cu-rich nanoprecipitates. Undoubtedly this deserves further investigations. Of particular importance would be to explore the impact of the Cu-rich precipitates on the mechanical properties of the

SGI for optimizing the structure–property relationships in line with recent efforts made in this respect.[28]

Conclusions

TEM examination showed the presence of Cu-rich particles in a pearlitic SGI alloyed with 0.82 wt%Cu. Particles of between 10 and 60 nanometers were found in cementite and ferrite lamellae and at the ferrite/cementite interface. The distribution of precipitates was heterogeneous in the pearlitic matrix. This fact, in conjunction with the Thermo-Calc calculations, led the authors to propose three possible stages for the formation of the Cu-rich phase (check Figure 10). Stage 1 involves particle precipitation in austenite. Stage 2 implies its simultaneous precipitation in ferrite and cementite, during the formation of pearlite. Stage 3 entails the precipitation in ferrite. Stages 2 and 3 were also supported by DSC experiments and elemental diffusion calculations. It was concluded that the formation of precipitates during these stages is controlled by the chemical composition, in particular the concentration of Cu. As a result, it was possible to correlate the observed distribution of Cu-rich nanoprecipitates in SGI alloyed with low amounts of Cu to the local variations of Cu concentration that result from the solidification-induced microsegregation in the metal matrix. The results of this study suggest that the content of Cu should be limited to low concentrations in order to restrict the formation of precipitates to low temperatures during cooling and thus ensure a fine precipitate distribution.

The knowledge gained is relevant for designing future experiments that cast light on the effect of the size and dispersion of the Cu-rich nanoprecipitates on the SGI

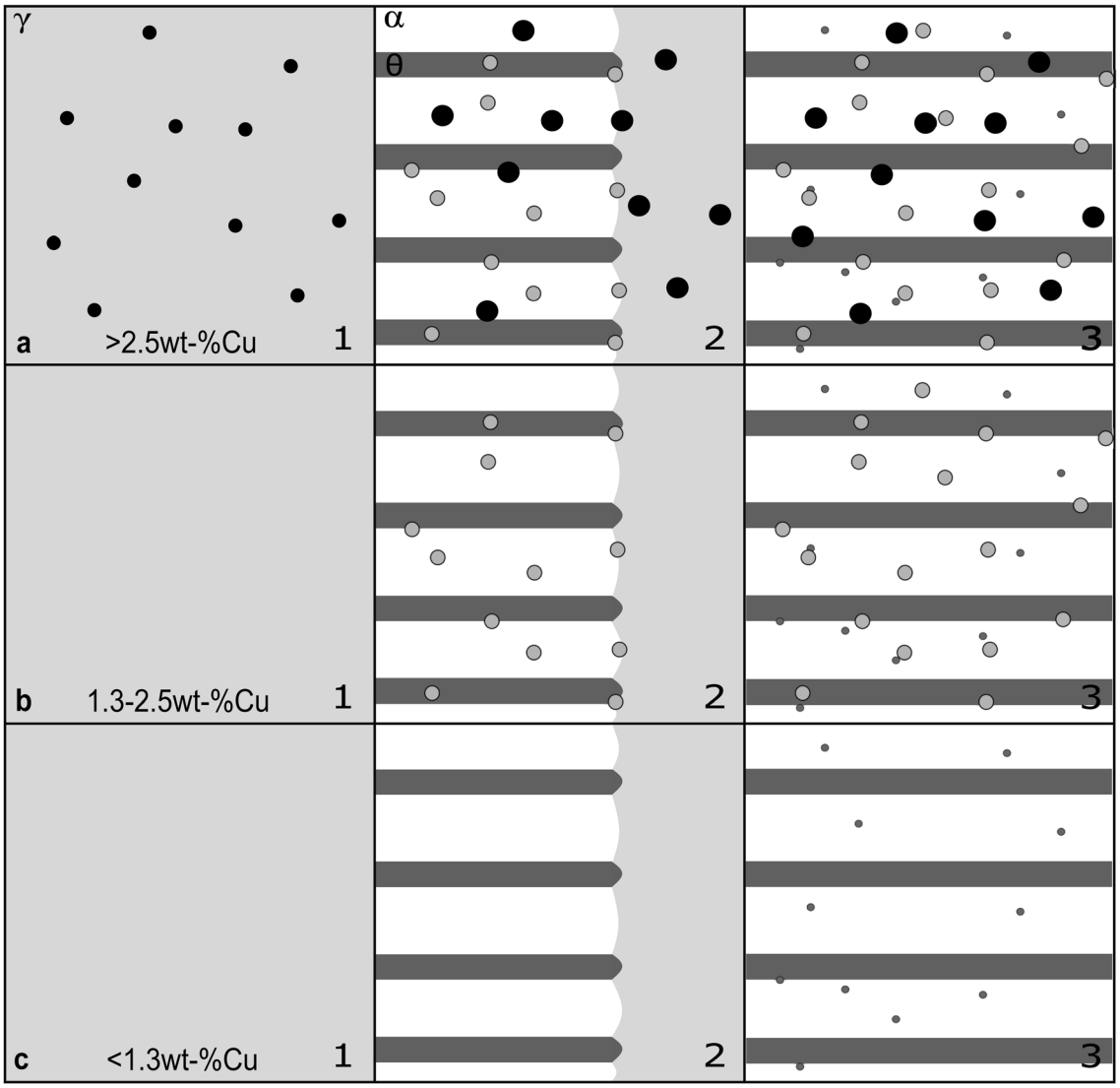

Figure 10. Three possible stages for the formation of the Cu-rich precipitates as proposed by the authors for the alloy under study: (a) for high, (b) medium and (c) low Cu concentrations.

strengthening as well as for optimizing the addition of alloying elements.

Acknowledgements

The authors would like to thank the Sánchez y Piccioni SA foundry for allowing the use of their facilities to produce the SGI samples.

Authors' contributions LNG and REB contributed to the study conception and design. Thermo-Calc simulations were designed and performed by RM. TEM measurements and image acquisitions were performed by LNG and AJT. EDS measurements were processed by MES. DSC experiment was designed by LNG and REB and performed by LNG. The first draft of the manuscript was written by LNG and REB, and all authors commented on previous versions of the manuscript. All authors read and approved the final manuscript.

REFERENCES

1. K. Lu, Science **28**, 328 (2010)
2. M.E. Fine, D. Isheim, Scr. Mater. **53**, 115 (2005)
3. Z. Jiao, J. Luan, M.K. Miller, C. Yu, C.T. Liu, Sci. Rep. **6**, 1 (2016)
4. Z.W. Zhang, C. Liu, M. Miller, X. Wang, Y. Wen, T. Fujita, A. Hirata, M. Chen, G. Chen, B. Chin, Sci. Rep. **3**, 1 (2013)
5. P. Othen, M. Jenkins, G. Smith, Philos. Mag. A **70**, 1 (1994)
6. Z. Jiao, J. Luan, Z.W. Zhang, M. Miller, W. Ma, C. Liu, Acta Mater. **61**, 5996 (2013)
7. I. Bataev, N. Stepanova, A. Bataev, A. Nikulina, A. Razumakov, Phys. Metals Metallogr. **117**, 901 (2016)
8. A.A. Razumakov, N.V. Stepanova, I.A. Bataev, O. Lenivtseva, I. Riapolova, K. Emurlaev, I.O.P. Conf, Ser. **124**, 1 (2016)
9. I.A. Bataev, N.V. Stepanova, A.A. Bataev, A.A. Razumakov, Russ. Phys. J. **60**, 1017 (2017)
10. A.A. Bataev, N.V. Stepanova, I.A. Bataev, Y. Kang, A. Razumakov, Met. Sci. Heat Treat. **60**, 150 (2018)
11. E.N. Pan, M.S. Lou, C.R. Loper, AFS Trans. **95**, 819 (1987)
12. J. Lacaze, A. Boudot, V. Gerval, D. Oquab, J. Lacaze, H. Santos, Metall. Mater. Trans. A **28**, 2015 (1997)
13. J. Lacaze, J. Sertucha, L. Magnusson Åberg, ISIJ Int. **9**, 1606 (2016)
14. J. Sertucha, P. Larrañaga, J. Lacaze, M. Insausti, Int. Metalcast. **4**, 51 (2010). https://doi.org/10.1007/BF03355486
15. J. Lacaze, Inter. Metalcast. **11**, 44 (2017)
16. L.N. García, A.J. Tolley, F.D. Carazo, R.E. Boeri, Mater. Sci. Technol. **35**, 2252 (2019)
17. A. Freulon, P. de Parseval, C. Josse, J. Bourdie, J. Lacaze, Metall. Mater. Trans. A **47**, 5362 (2016)
18. H.D. Machado, R. Aristizabal-Sierra, C. Garcia-Mateo, I. Toda-Caraballo, Int. J. Metalcast. **14**, 836 (2020). https://doi.org/10.1007/s40962-020-00450-1
19. R.E. Boeri, F. Weinberg, AFS Trans. **97**, 179 (1989)
20. J.O. Andersson, T. Helander, L. Höglund, P. Shi, B. Sundman, Calphad **26**, 273 (2002)
21. L.A. Currie, Anal. Chim. Acta **391**, 127 (1999)
22. R. Ivanova, W. Sha, S. Malinov, ISIJ Int. **44**(5), 896 (2004)
23. V. Gerval, J. Lacaze, ISIJ Int. **40**, 386 (2000)
24. J. Eiken and J. Lacaze, in 6th Decennial International Conference on Solidification Processing (2017)
25. M. Murakami, Y. Takanaga, N. Nakada, T. Tsuchiyama, S. Takaki, ISIJ Int. **48**, 1467 (2008)
26. R.F. Mehl, W.C. Hagel, Prog. Met. Phys. **6**, 74 (1956)
27. J. Fridberg, L.E. Torndahl, M. Hillert, Jernkont. Ann. **153**, 263 (1969)
28. J.M. Tartaglia, R.B. Gundlach, G.M. Goodrich, Int. Metalcast. **8**, 7 (2014). https://doi.org/10.1007/BF03355592